









Cite this: *CrystEngComm*, 2019, 21, 2768

## The origin of the unusual DSC peaks of supercooled barium disilicate liquid†

Benjamin J. A. Moulton, \*<sup>ab</sup> Alisson M. Rodrigues, <sup>b</sup> David V. Sampaio, <sup>ab</sup> Laís D. Silva, <sup>b</sup> Thiago R. Cunha, <sup>a</sup> Edgar D. Zanotto <sup>b</sup> and Paulo S. Pizani <sup>ab</sup>

It is known that barium disilicate (BS2) glass exhibits two prominent exothermic peaks between the glass transition and melting temperatures in calorimetric experiments, however, their cause is not known. In this work, glass-ceramic samples were produced inside a differential scanning calorimeter (DSC) and then investigated *ex situ* with X-ray diffraction (XRD) and Raman spectroscopy. We found that the first exothermic peak results from multiphase crystallization although a signature of residual glass is still observed. H-BaSi<sub>2</sub>O<sub>5</sub>, and Ba<sub>3</sub>Si<sub>5</sub>O<sub>13</sub> were directly identified after the first exothermic peak, however, both L-BaSi<sub>2</sub>O<sub>5</sub> and an unknown phase(s) are also formed. Rietveld analysis indicates <1% Ba<sub>3</sub>Si<sub>5</sub>O<sub>13</sub> in the sample heat treated at 853 °C (the first exothermic peak maximum). Amorphous halos are observed in the XRD patterns of samples heated to temperatures until the second exothermic peak. Raman spectra suggest that the crystalline phases are somewhat distorted or contain defects. The second exothermic peak is actually a composite peak composed of two contributions. We interpret these shoulders as separate processes including crystallization of non-stoichiometric phases, crystallization of the residual glass, and the phase transition of monoclinic H-BaSi<sub>2</sub>O<sub>5</sub> to orthorhombic L-BaSi<sub>2</sub>O<sub>5</sub>. After the second exothermic peak, the XRD and Raman spectra show that the samples have become L-BaSi<sub>2</sub>O<sub>5</sub>. These results clarify the relationships between thermal history and crystalline phase formation, which may be used to produce glass-ceramics with desirable properties.

Received 3rd December 2018,  
Accepted 14th March 2019

DOI: 10.1039/c8ce02054j

rsc.li/crystengcomm

## 1 Introduction

Barium disilicate (BS2 – BaSi<sub>2</sub>O<sub>5</sub>) is an interesting, unusual glass-forming composition due to it being one of very few compositions that experiences internal crystal nucleation without a nucleating agent.<sup>1–5</sup> BS2-based glass and glass-ceramics are important as solid oxide fuel cell sealants (*e.g.* ref. 6) and, when properly doped, show enhanced luminescence.<sup>7</sup> BS2 glass is also known to crystallize both polymorphs of BS2, the low, orthorhombic sanbornite (L-BS2) and the high, monoclinic form (H-BS2). Despite being a stoichiometric composition, along with fresnoite (Ba<sub>2</sub>TiSi<sub>2</sub>O<sub>8</sub>) and diopside (CaMgSi<sub>2</sub>O<sub>6</sub>), BS2 glass shows a second exothermic peak its DSC patterns.<sup>8–10</sup> These two peaks have often been inferred to be the crystallization of H-BS2 and recrystallization to L-BS2,<sup>7</sup> however, in light of several recent studies, which have found non-stoichiometric phases during the early stages

of crystallization, their cause is in doubt. This study aims to clarify the origin of these DSC peaks by a careful determination of the phases produced during each of these peaks.

Early studies concluded that the supercooled liquid (SCL) BS2 displayed nucleation of a small (<10 nm) spherical precursor phase, identified as monoclinic BS2 (H-BS2), when heat treated for <40 h at the temperature of the maximum nucleation rate, 700 °C.<sup>1,2</sup> When heat treated for longer times, 40–116 h, larger needle growths appeared consisting of a central axial spine with epitaxial growth of fibrils along the spines. These axial spines were identified as orthorhombic sanbornite (L-BS2), whereas the fibrillar side growths were identified as the high temperature phase, monoclinic BS2 (H-BS2).<sup>1,2</sup>

The presence of non-stoichiometric phases has been observed in BaSi<sub>2</sub>O<sub>5</sub> ceramics prepared under varying synthesis conditions (*e.g.* ref. 11 and 12). More recent studies have suggested that a non-stoichiometric phase, Ba<sub>5</sub>Si<sub>8</sub>O<sub>21</sub>, is in fact the initial nucleating phase from which H-BS2 grows (*e.g.* ref. 13 and 14). To further complicate the crystallization process, the presence of residual glass has recently been found even after the second exothermic peak when L-BS2 is already the dominant phase.<sup>15</sup> In fact, the presence of interstitial glass between the arms of spherulitic crystals has led

<sup>a</sup> Universidade Federal de São Carlos, Departamento de Física, Rod. Washington Luís, Km 235 13565-905 São Carlos, SP, Brazil. E-mail: benmoul@df.ufscar.br

<sup>b</sup> CERTEV — Center for Research, Technology, and Education in Vitreous Materials, Department of Materials Engineering, Federal University of São Carlos, 13565 - 905 São Carlos, SP, Brazil, Web: www.certeve.ufscar.br

† Electronic supplementary information (ESI) available. See DOI: 10.1039/c8ce02054j

to large discrepancies between the volume fraction of crystals determined from X-ray diffraction (XRD) and optical microscopy, where the latter method grossly overestimates the fraction.<sup>4</sup> The presence of residual glass, non-stoichiometric phases, and a polymorphic phase transition provide many possibilities for the origin of the exothermic peaks observed in the DSC patterns of this glass.

BS2 glass typically has two exothermic peaks at 850 °C and 905 °C when heating at 10 °C min<sup>-1</sup> by DSC.<sup>5,15–17</sup> Time-dependent studies have parameterized these peaks in order to estimate the steady-state nucleation rate, as well as, other properties.<sup>18</sup> Based on the results of Ramsden and James,<sup>2</sup> Silva *et al.*,<sup>16</sup> assumed that these peaks correspond to the formation of H-BS2 and the phase transition to L-BS2, respectively. This is consistent with the results of Oehlschlegel.<sup>19</sup> However, this interpretation is challenged by the evidence for the involvement of non-stoichiometric phases in the early stages of crystallization. The original interpretation Ramsden and James<sup>2</sup> has informed much of the recent developments on homogeneous crystal nucleation theories.<sup>20,21</sup> Such developments have resulted in several empirical relationships between glass structure and homogeneous nucleation.<sup>22,23</sup> However, these conclusions are predicated on the importance of stoichiometry and volume nucleation of BS2 glass.

From the above studies we hypothesize several plausible interpretations for the origin of these two peaks, the possible explanations for their origin are: a) crystallization of H-BS2 followed by a phase transition to L-BS2 (*e.g.* ref. 2); b) mixed crystallization of a non-stoichiometric phase and H-BS2 followed by recrystallization and the high-to-low phase transition (*e.g.* ref. 14); or, c) incomplete crystallization followed by complete crystallization and phase transition (*e.g.* ref. 15). Once the origin of these two exothermic peaks is clarified, this information may be used to design glass-ceramics by, potentially, stabilizing a given polymorph of known properties (*e.g.* high thermal expansion coefficients or chemical durability).

The goal of this study is to ascertain the origin of these two, or three, exothermic peaks (Fig. 1) and to gain insight into the presence of metastable precursor phases, whether stoichiometric or not. To achieve our goal, a series of BS2 glass samples were measured after being heat treated in the DSC to different maximum temperatures and also isothermally treated up to 8 hours (480 min). The isothermal treatments were carried out at temperatures chosen to isolate the crystal phases which are produced during each of these exothermic peaks. These samples were then analyzed using X-ray diffraction (XRD) and Raman spectroscopy to identify the phases formed under the different temperature–time regimes.

## 2 Experimental procedures

The details of our glass synthesis have been previously reported by Rodrigues *et al.*<sup>5,24</sup> and we summarize their preparation here. High purity reagents of BaCO<sub>3</sub> and SiO<sub>2</sub> were

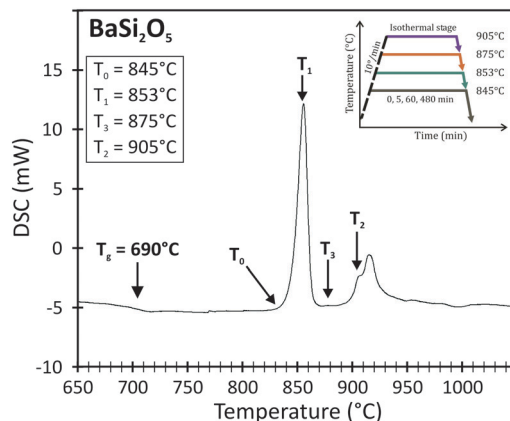


Fig. 1 Non-isothermal DSC curve of BS2 heated at 10 °C min<sup>-1</sup>. Temperatures correspond to the onset of the first exothermic peak ( $T_0 = 845$  °C), the first exothermic peak maximum ( $T_1 = 853$  °C), the completion of the first peak ( $T_2 = 875$  °C), and the local maximum of the second exothermic peak ( $T_3 = 905$  °C). The inset figure shows the temperature–time paths of the samples produced inside the DSC.

mixed and placed in a platinum crucible for calcined for 36 hours at 1350 °C and then melted at 1550 °C for 30 min; the liquid obtained was poured on steel plate and re-melted three more times to homogenize and prevent the formation of streaks. In the last re-melting, the liquids were pressed between two steel plates (splat-cooling), and inserted in a furnace for annealing at a temperature 90 °C below its glass transition temperature ( $T_g - 90$  °C) to permit cutting. The BS2 glass used here is the same as our previous study which had a mean composition of 33.8BaO–66.2SiO<sub>2</sub> based electron probe microanalyzer (EPMA) results.<sup>25</sup>

The experimental procedures were designed to isolate the first and second exothermic peaks. All differential scanning calorimetric (DSC) experiments were performed in a NETZSCH STA 449C thermal analyzer using platinum crucibles in air. Cubic vitreous samples (~45 mg) were heated up by 10 °C min<sup>-1</sup> from room temperature until the complete melting peak appeared. Once the  $T_g$ , onset and peak temperatures of the first and second peaks, and the melting temperature were identified, the experimental procedure was designed as follows: vitreous samples were heated up at 10 °C min<sup>-1</sup> from room temperature until near the onset temperature of the first exothermic peak ( $T_0 = 845$  °C) and immediately cooled to room temperature at 50 °C min<sup>-1</sup>. This procedure was repeated three more times: first, the sample was stopped at the temperature of the first exothermic peak maximum ( $T_1 = 853$  °C); second, the sample was stopped between the first and second exothermic peaks ( $T_2 = 875$  °C); and third, the sample was stopped after the second exothermic peak maximum ( $T_3 = 905$  °C). Also, at each of these temperatures,  $T_{0-3}$ , isothermal heat treatments were done, ranging in time between 5 to 480 min (Fig. 1).

The Raman spectroscopy measurements used either a 532 nm, or 633 nm, excitation wavelength applying 8 mW, or ~2 mW, on the sample, respectively. All spectra were taken at room temperature using either 100× or 50× (long working

distance) objective with either 1800 gr mm<sup>-1</sup> or 600 gr mm<sup>-1</sup> gratings. Only spectra taken using the 1800 gr mm<sup>-1</sup> grating are described as 'high resolution' as they have a resolution close to 1 cm<sup>-1</sup>. The spectrometer was calibrated against the silicon peak position at 520.7 cm<sup>-1</sup>. Each sample was analyzed 6 or more times on both the top and side surfaces, as well as, broken apart and analyzed on a fresh internal fracture surface of the sample. Reported below are representative spectra taken from a total of >100 spectra. Curve fitting of the Raman spectra was carried out after removing a polynomial background which was anchored where the laser line intersected with the spectrum as well as the flat regions around 700 and 1300 cm<sup>-1</sup>. Curve fits used Lorentzian lineshapes to reproduce the spectral envelope in the Fityk program.<sup>26</sup>

XRD measurements were done using a Rigaku Ultima IV diffractometer with Cu K $\alpha$  radiation ( $\lambda = 0.1541$  nm). Diffractograms were recorded in continuous scanning mode at a rate of 0.5° min<sup>-1</sup> in steps of 0.02° collected in the range 10°  $\leq 2\theta \leq 80^\circ$ . Rietveld refinement of the diffractograms used the GSAS software package.<sup>27,28</sup> The results below are considered to be of high quality because the  $R$  values are <10% and the goodness of fit ( $S = R_{\text{weighted-profile}}/R_{\text{expected}}$ ) remains close to 1.<sup>29</sup>

For clarity, the nomenclature throughout the paper follows the molar ratios of BaO:SiO<sub>2</sub>. For example, barium disilicate composition, BaSi<sub>2</sub>O<sub>5</sub>, is referred to as BS2. The low (orthorhombic sanbornite) and high (monoclinic) polymorphs are therefore L-BS2 and H-BS2, respectively. The non-stoichiometric phases Ba<sub>3</sub>Si<sub>5</sub>O<sub>13</sub> and Ba<sub>5</sub>Si<sub>8</sub>O<sub>21</sub> are referred to as B3S5 and B5S8, respectively. The ICSD files used to identify these phases are those from ref. 30 and 31: H-BS2 – 100314, L-BS2 – 100313, B3S5 – 100312, and B5S8 – 100311. The synthetic samples of L-BS2 and H-BS2 were made from a BS2 glass using the heat treatment described in ref. 12. Synthetic samples of B3S5 and B5S8 were provided by Gorelova *et al.*,<sup>12</sup> All standards were confirmed by XRD using the ICSD database.

## 3 Results

### 3.1 DSC results

Fig. 1 shows part of the DSC curve at 10 °C min<sup>-1</sup> to BS2 glass.  $T_g$  was determined to be 690  $\pm$  2 °C by the tangent method.<sup>32,33</sup> The melting temperature ( $T_m$ ) obtained was 1420  $\pm$  2 °C. These values are in agreement with other studies on BS2 glass.<sup>9,20</sup> In addition, two distinct exothermic peaks are observed on range temperature between  $T_g$  and  $T_m$ . The two exothermic peaks have local maxima at 853 °C ( $T_1$ ) and 905 °C ( $T_3$ ). The second exothermic peak is actually a composite peak with a second local maximum at 915 °C (Fig. 1).

Fig. 2 shows example DSC patterns for the isothermal heat treatments at 875 °C (Fig. 2A) and 905 °C (Fig. 2B). All of the conditions between the isothermal and non-isothermal are the same until the temperature of interest is reached. Therefore, the first exothermic peak is sharp and intense, and

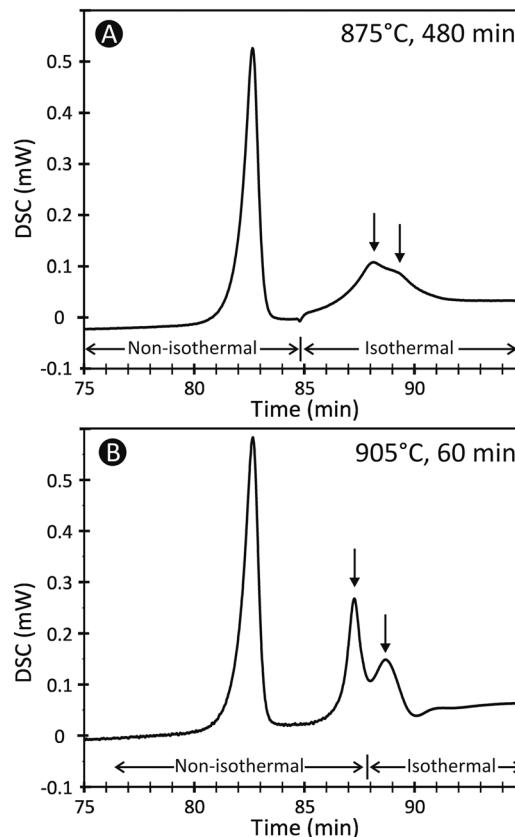
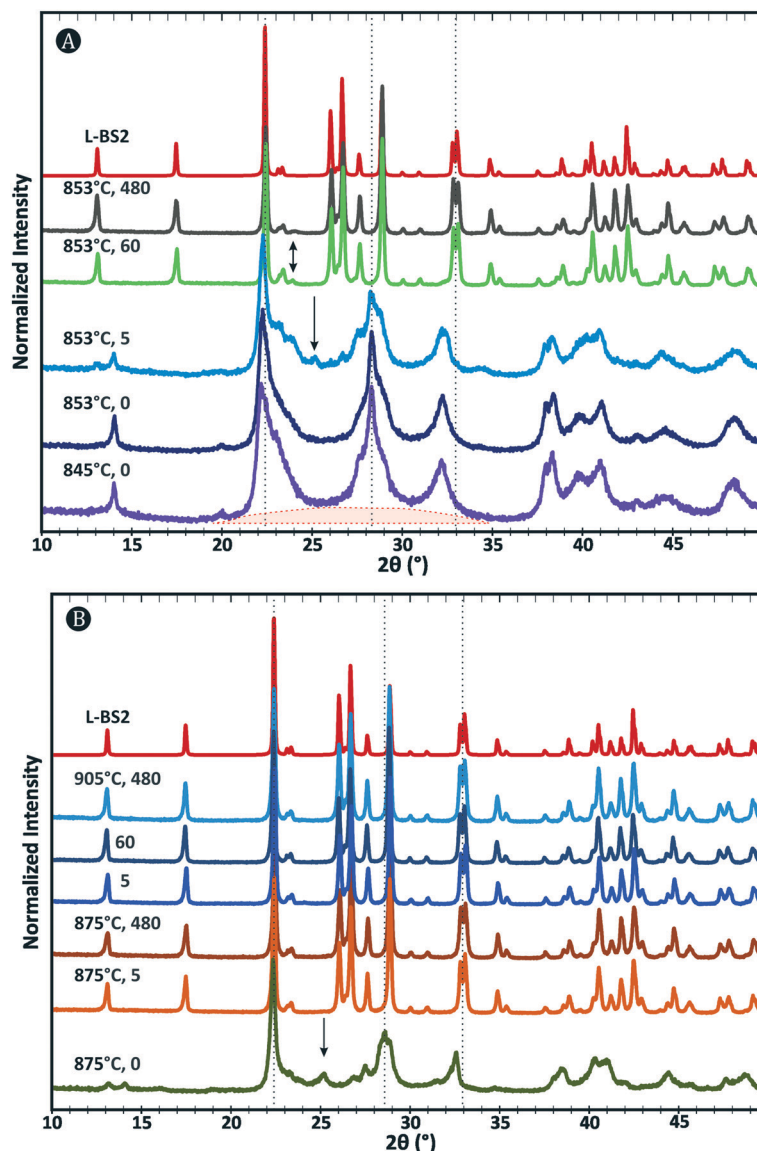


Fig. 2 Example isothermal DSC pattern of A)  $T_2$  – 875 °C, 480 min, and B)  $T_3$  – 905 °C, 60 min samples. Note that two distinct shoulders (arrows) are observed in the second exothermic peak.

found at the same time in both examples. In contrast, the two maxima observed in the second exothermic peak (Fig. 1) may become more or less distinct depending on the specific heat treatment. This can be seen in Fig. 2 which shows the isothermal heat treatments at the DSC temperature at 875 °C (480 min) and 905 °C (60 min).

### 3.2 X-ray diffraction results

Regardless of the temperature–time treatment, all diffractograms show an intense peak found at 22.5° (Fig. 3). When quenched (0 min) from either 845 or 853 °C, the diffractogram displays additional peaks which are considerably broad and often asymmetric (Fig. 3A). These samples display quite broad and asymmetric peaks that did not yield a unique solution to the Rietveld analysis. In the diffractogram of the 845 °C, 0 min sample there are several regions with broad nonlinear background contributions. The most intense background is observed between 23 and 32°  $2\theta$  (orange region, Fig. 3A). At higher temperatures these background contributions are considerably reduced but still remain in the diffractograms (e.g. 875 °C, 0 min sample in Fig. 3B). The most intense background contribution is lost after 60 min at 853 °C or 5 min at 875 °C. At 853 °C, 5 min, however, the diffractogram shows the development of



**Fig. 3** Diffractograms of BS2 glass held at  $T_0$  and  $T_1$  (A), and at  $T_2$  and  $T_3$  (B). Note that the two exothermic peak maxima are at 853 °C ( $T_1$ ) and 905 °C ( $T_3$ ). At the top of both figures is the ICSD diffractogram for orthorhombic L-BS2 (no. 100313). Vertical dotted lines indicate the  $2\theta$  ranges 22.5°, 28.5° and 33°. Curved orange area (color online) below the 845 °C, 0 min, pattern highlights the ‘amorphous halo’ described in the text. In the bottom (B) figure, the 5 and 60 refer to the 905 °C held for 5 and 60 min, respectively.

distinct peaks at 23°, 24°, and 25°  $2\theta$  as well as distinct shoulders within the broad feature found between 28° and 32°  $2\theta$  (Fig. 3A). While there are other distinctions between the diffractograms, the above features will suffice as evidence for the discussion below.

### 3.3 Raman spectra

As with the XRD results above, the Raman spectra are divided between those samples produced at 845 °C and 853 °C (Fig. 4A) and those at 875 °C and 905 °C (Fig. 4B). In all spectra, the most intense bands are found near 530 and 1075  $\text{cm}^{-1}$ . In general, as the temperature or time increase, the Raman bands have a smaller full-width at half-maximum

(FWHM) and have increasingly sharper peaks in the low frequency shift range ( $<500 \text{ cm}^{-1}$ ). For example, the samples produced at either 845 or 853 °C, 0 min show a doublet centered around 550  $\text{cm}^{-1}$  that becomes a sharp singlet after 60 min at 853 °C (Fig. 4A). There are also clear distinctions in the low frequency region where the sample from 845 and 853 °C, 0 min has a distinct quadruplet found between 250 and 330  $\text{cm}^{-1}$  whereas the 853 °C, 60 min sample shows a distinct doublet at 330  $\text{cm}^{-1}$  as well as sharp peaks at 191 and 223  $\text{cm}^{-1}$ . Similar changes are evident in the sample heat treated at 875 °C (Fig. 4B).

In contrast, the spectra of the 853 °C, 60 min sample (Fig. 4A), the 875 °C, 480 min sample, and all spectra taken of samples treated at 905 °C (Fig. 4B) show the doublet at

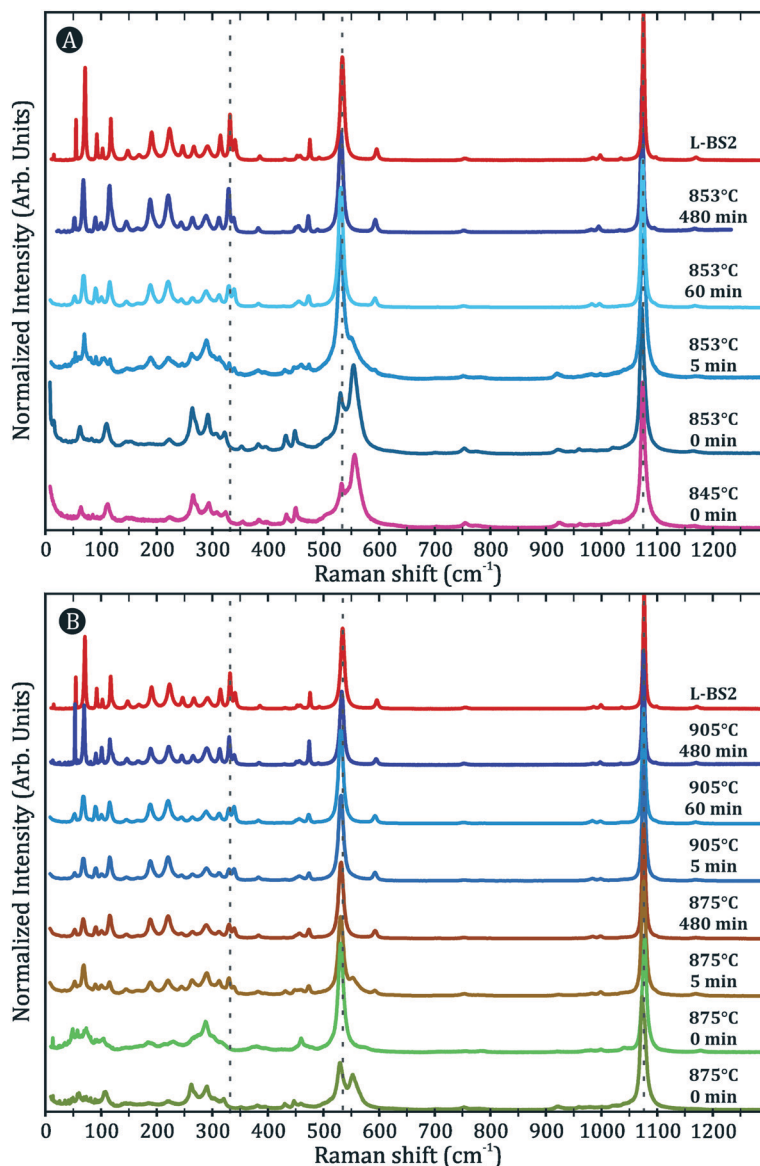


Fig. 4 Representative Raman spectra of BS2 glass samples. Low temperature (A) and high temperature (B) spectra as labeled. At the top of each panel is the synthetic L-BS2 (orthorhombic BaSi<sub>2</sub>O<sub>5</sub>) spectrum. Note all spectra taken at 60 min or 480 min are essentially identical to the L-BS2 standard. The two spectra taken at 875 °C, 0 min, are two high resolution analyses taken from different regions from a 'fresh' fractured surface within the sample.

330 cm<sup>-1</sup> and intense, sharp peaks at 533 cm<sup>-1</sup> and 1076 cm<sup>-1</sup>. Although subtle, the latter two peaks show slight, positive shifts of +2 cm<sup>-1</sup> from their position in the spectra taken from samples heat treated for only 0 or 5 min (Table 1).

## 4 Discussion of the origins of the exothermic DSC peaks

### 4.1 What is the origin of the 1<sup>st</sup> DSC peak?

To describe the phases formed during the first peak the 0 min samples quenched immediately from 845 °C to 875 °C are most informative. Of the three 0 min diffractograms, the 875 °C sample displays the sharpest Bragg peaks, whereas the peaks in the 845 °C and 853 °C patterns are considerably

broader and have larger background contributions (Fig. 5). The main diffraction peak, at 22–23°, in all diffractograms can be assigned either to the [310] plane of H-BS2, or, the [011] plane of L-BS2.<sup>31</sup> There is only a small separation of these peaks by 0.10°, where the [011] peak of L-BS2 is centered at 22.40° 2θ, slightly above that of the [310] peak, which makes the use of these peaks to distinguish between these polymorphs difficult. In fact, H-BS2 is best identified by the peak 25.7° 2θ corresponding to the [602] plane as well as the set of planes ([602], [204], and [404]) found between 28 and 29° 2θ, which are evident in the 853 °C, 5 min (arrow in Fig. 3A) and 875 °C, 0 min diffractograms (Fig. 5). Thus, H-BS2 is produced during the first exothermic peak. However, due to the broad peaks present in our data and the

**Table 1** Peak parameters of curve fits for short times ( $t = 0$  & 5 min at 845, 853, and 875 °C), long times ( $t = 60$  & 480 min for all temperatures) and synthetic L- and H-BS2

Short times			Long times			L-BS2 <sup>b</sup>			H-BS2 <sup>c</sup>			Assignment	Note	
Parameter	$n^a$	Mean	std. dev	$n$	Mean	std. dev	$n$	Mean	std. dev	$n$	Mean			std. dev
Center	27	530.8	0.7	17	532.7	1.0	4	535.2	0.3	7	533.5	0.2	Si–O–Si bend	1st peak in 550 doublet
FWHM		12.9	1.7		9.4	0.7		8.5	0.1		8.8	0.1		
Center	25	554.2	1.0										?Si–O–Si bend	2nd peak in 550 doublet
FWHM		18.8	2.2											
Center	23	1074.2	0.8	17	1076.3	1.1	4	1076.8	0.1	7	1079.2	0.1	NBO–Si stretch	1075 main, intense peak
FWHM		8.9	1.6		5.8	0.8		4.6	0.1		5.4	0.2		
Center	17	1079.3	2.3										?NBO–Si stretch	1080 secondary, weak peak
FWHM		14.6	5.8											

<sup>a</sup>  $n$  is the number of spectra used in the determination. <sup>b</sup> L-BS2 values comes from both synthetic and natural (sanbornite) L-BS2. Natural sanbornite was from the Royal Ontario Museum (ROM) sample no. M24323. <sup>c</sup> H-BS2 mean values come from both in-house synthetic H-BS2 as well as the BS2 from Gorelova *et al.*<sup>12</sup>

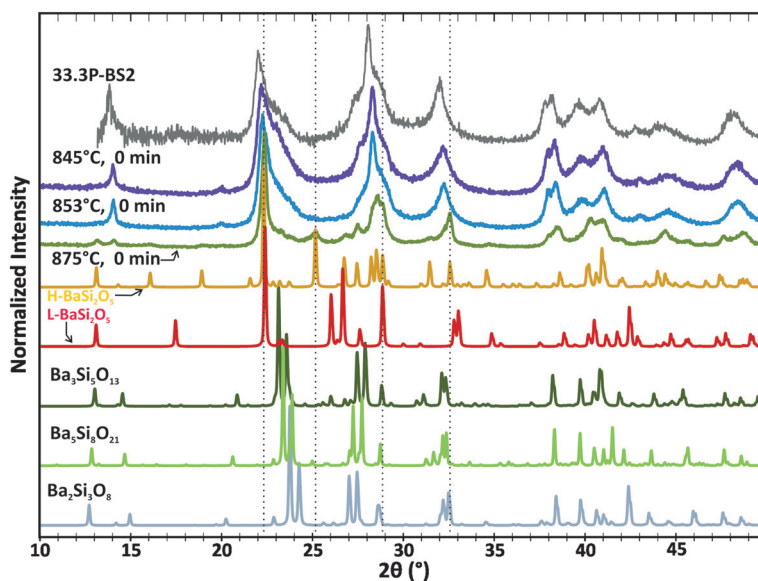


**Fig. 5** Comparison of the XRD patterns for samples immediately quenched from the 845 °C, 853 °C, and 875 °C with ICSD database diffractograms of L-BS2 (100313), H-BS2 (100314), Ba<sub>3</sub>Si<sub>5</sub>O<sub>13</sub> (100312), Ba<sub>5</sub>Si<sub>8</sub>O<sub>21</sub> (100311) and Ba<sub>2</sub>Si<sub>3</sub>O<sub>8</sub> (100310). Parentheses indicate the ICSD crystal code. Dashed lines are placed key peaks used to identify H-BS2 in the samples. All patterns have been intensity normalized to one. 33.3P-BS2 is a nearly stoichiometric BS2 glass from (Zanotto, 1982).<sup>34</sup>

similarities between the two polymorphic phases, the Rietveld analysis is not conclusive. Therefore, we cannot eliminate the formation of L-BS2 during the first exothermic peak.

In addition, the 22° peak is always asymmetric to higher  $2\theta$  values. In the diffraction pattern of 875 °C, 0 min this asymmetry develops into peaks at 23.10° and 23.50° as well as a new peak which appears near 27°, which are indicative of the non-stoichiometric phase B3S5 (Fig. 5). The presence of B3S5 is confirmed by Rietveld analysis of the 853 °C samples which require ~1% of B3S5 for samples held for 60 and 480 min (ESI† Fig. S1). This small amount of B3S5 is consistent with the fact that the glass used in this study is not perfectly stoichiometric; it is actually slightly baria-rich (33.8 rather than 33.33 mol% BaO). However, the slight difference in stoichiometry cannot explain the fact that it is not found in the glasses treated at 875 °C or 905 °C for 5 min. More-

over, the slight imperfection in stoichiometry cannot explain the breadth and intensity of diffraction peaks between 22° and 24°  $2\theta$  found consistently in the diffractograms of the samples quenched (0 min) from the temperature of the local maximum of its second exothermic peak;  $T_{3\text{-Pure}} = 910$  °C, 0 min. The Raman spectra (not shown) and diffractogram (Fig. 5; sample 33.3P-BS2) are indistinguishable from the results of BS2 glass used herein. Therefore, we conclude that stoichiometry is not the source of this behavior.

Moreover, we tested this result to see if the non-stoichiometric phases formed in a 'pure' stoichiometric BS2 glass (33.3 mol% BaO, 0.004 mol% SrO) from ref. 34. A sample of this glass was produced in the same manor as above by quenching it from the temperature of the local maximum of its second exothermic peak;  $T_{3\text{-Pure}} = 910$  °C, 0 min. The Raman spectra (not shown) and diffractogram (Fig. 5; sample 33.3P-BS2) are indistinguishable from the results of BS2 glass used herein. Therefore, we conclude that stoichiometry is not the source of this behavior.

The presence of B3S5 was also reported in another (nominally) BS2 glass heat treated for 60 min at 950 °C.<sup>7</sup> This apparent discrepancy in temperature may be explained by the

difference in sample size which in the former study was “2 cm<sup>2</sup> disks” whereas our samples are a fraction of the size, ~2 mm<sup>3</sup>. Therefore, the sample mass (volume) is a critical factor that should be reported for all calorimetric and kinetic studies. Nevertheless, the first exothermic DSC peak clearly involves the crystallization of at least one non-stoichiometric phase.

A broad background contribution is found between 23 and 32° 2θ. In ionic liquids, these broad contributions have been described as amorphous halos<sup>35,36</sup> and broad features at low momentum transfer have long been known in glasses.<sup>37,38</sup> Converting the scattering angles to real space distances this background contribution appears to be derived from intermediate range structural order on the scale of 2.8–3.8 Å. This distance correlates to the range of Ba–O bond lengths in the BS2 polymorphs, which spans 2.7–3.2 Å.<sup>30,31</sup> While an amorphous halo is prominent in the 845 °C, 0 min diffractogram, it is fainter, although still present, in the 875 °C, 0 min pattern (Fig. 5). Therefore, the presence of the amorphous halo indicates that there is some residual glass remaining after the first exothermic peak. This lends credence to the reported residual glass found at 1100 °C using transmission electron microprobes.<sup>15</sup>

Although no signature of B3S5 nor other non-stoichiometric barium silicate phases were found in the Raman spectra, it was not likely given the small fractions expected and the local nature of the Raman probe. However, Raman spectra do show several systematic changes with increasing temperature and time. In general, as the temperature and time increase the vibrational bands become sharper and shift to slightly higher frequency (Fig. 6). The most intense Raman bands in simple binary silicate minerals (M<sub>2</sub>O–SiO<sub>2</sub> or MO–SiO<sub>2</sub>, where M = Na, Ba, etc.) of the meta-

to di-silicate compositions are the Si–O–Si bending (500–700 cm<sup>-1</sup>) and symmetric stretching (900–1100 cm<sup>-1</sup>) vibrational modes of the SiO<sub>4</sub> tetrahedron.<sup>39,40</sup> Both spectra of H-BS2 and L-BS2 show sharp peaks with FWHM of <9 cm<sup>-1</sup> and <6 cm<sup>-1</sup> for the bending and stretching modes, respectively (Table 1). In contrast, the FWHM of the bending and stretching modes for 0 min samples heated from 845 °C to 875 °C have mean values of 12.9 cm<sup>-1</sup> and 8.9 cm<sup>-1</sup>, respectively (Table 1). The FWHM corresponds to the lifetime of the vibrational mode which becomes shorter as a result of dephasing, or destructive interference between vibrations of similar frequency (*cf.* ref. 41). As the FWHM decreases as the temperature and time of the heat treatments increase, it seems that the crystal structures become better developed at longer time and higher temperatures (Fig. 7). This narrowing of the FWHM is expected because the initial crystals observed in BS2 are fibrillar and spherulitic.<sup>1,2,24</sup> The narrowing may also be related to the small size, distortion, or preferential orientation of the crystal growth. In part, this may also explain the lack of, and breadth of, the Bragg peaks in the XRD patterns. Unfortunately, more is not known about the characteristic behaviors of these vibrations. However, the broadening is apparent in both bending and stretching modes indicating some deviation from the single crystal structure and possibly some distortion of the SiO<sub>4</sub> tetrahedra.

The other major feature observed in our Raman spectra is the 550 doublet in the Si–O–Si bending mode with local maxima at 531 cm<sup>-1</sup> and 554 cm<sup>-1</sup> (Fig. 6 and 7). The general trend is that as the time and temperature of the heat treatment increase the intensity of the 530.8 cm<sup>-1</sup> peak increases whereas the intensity of the 554.2 cm<sup>-1</sup> peak decreases. Although this is generally the case, for any given temperature–time treatment the relative peak intensities do display

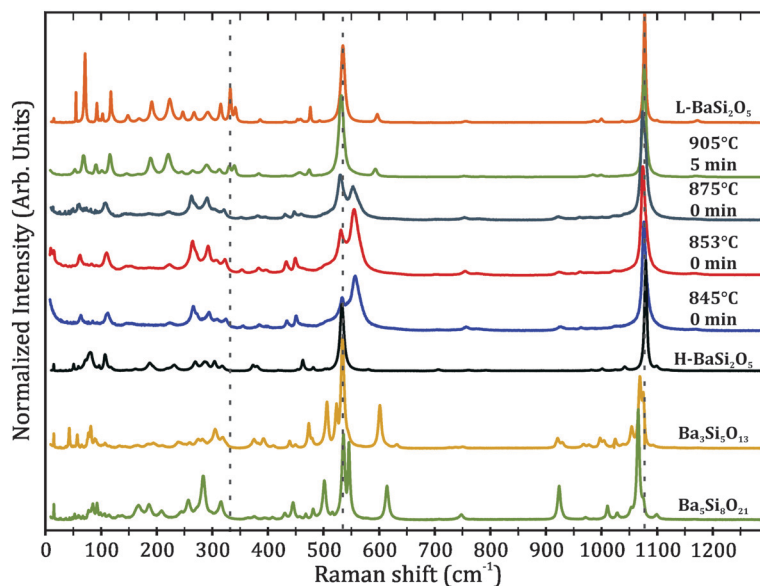
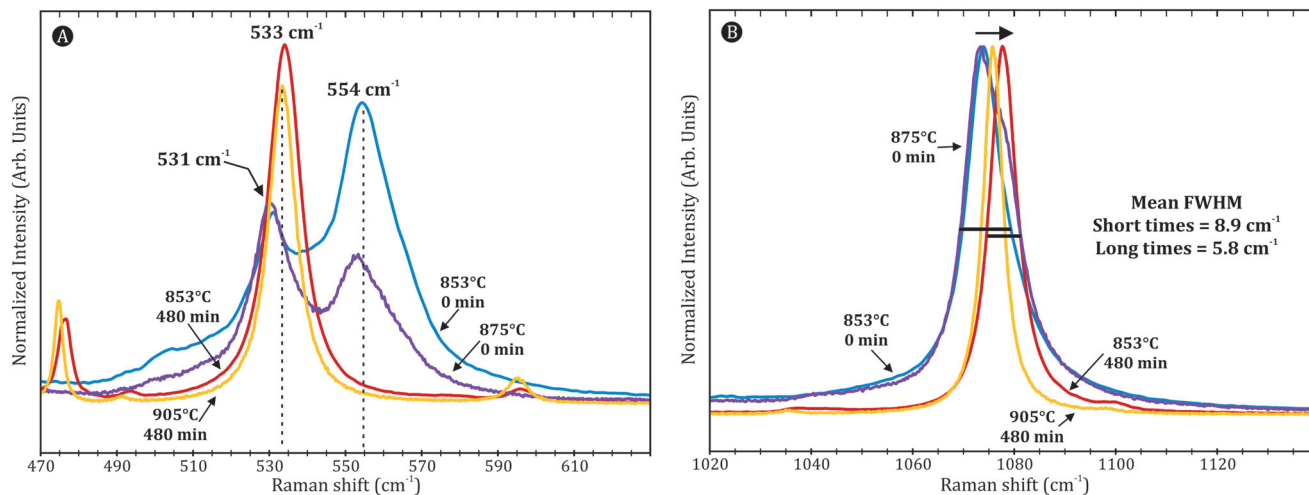


Fig. 6 Representative Raman spectra of run products and crystalline barium silicate standards for comparison. Dashed lines correspond to peaks in L-BS2 including the 330 cm<sup>-1</sup> doublet, the Si–O–Si bending mode at 535.2 cm<sup>-1</sup> and the symmetric stretch at 1076.8 cm<sup>-1</sup>. All patterns have been intensity normalized to one.



**Fig. 7** Representative spectra showing the evolution from A) short times at  $T_1$  and  $T_2$  (0 min at 853 °C and 875 °C) and long times at  $T_1$  and  $T_3$  (480 min at 853 °C and 905 °C) for the Si–O–Si bending mode ( $\sim 533\text{ cm}^{-1}$ ) on top and B) for the symmetric stretching mode near  $1075\text{ cm}^{-1}$  of the same samples on bottom. For both vibrational modes there is a positive shift with increasing time (Table 1). See text for discussion of the 550 doublet for the 0 min samples shown on top.

considerable variability. As noted above, in many sheet- (e.g., phyllosilicates including H-BS2) and chain-silicate (pyroxenes) minerals the intense band centered in the  $500\text{--}600\text{ cm}^{-1}$  range is assigned to Si–O–Si bending mode.<sup>42</sup> Although B5S8 does show a sharp doublet, the second peak is observed at  $546\text{ cm}^{-1}$  rather than  $554\text{ cm}^{-1}$  (Fig. 6). No other barium silicate standards show this doublet. Interestingly, in alkali disilicate minerals, this band is also split into a doublet.<sup>43</sup> In our spectra (Fig. 7), the FWHM is  $\sim 13\text{ cm}^{-1}$  for the first peak and  $\sim 19\text{ cm}^{-1}$  for the second,  $554\text{ cm}^{-1}$  peak (Table 1). Ultimately, this peak is characteristic of the early stages of crystallization in BS2 glass and is not characteristic of well formed non-stoichiometric phases. The breadth of these peaks suggests local disorder and may involve an additional symmetry element, for example, a change in symmetry or a twin plane. Doublets are known to form in the Si–O–Si bending and  $\text{SiO}_4$  symmetric stretching modes when there is a reduction in symmetry. For example, as Mg is substituted for Ca in the chain silicate series, diopside ( $\text{CaMgSi}_2\text{O}_6 - C2/c$ ) to enstatite ( $\text{Mg}_2\text{Si}_2\text{O}_6 - P2_1/C$ ) series.<sup>44</sup> However, this is not true of the polymorphic transition of H-BS2 to L-BS2. At present an explanation for the 550 doublet remains elusive, however, the 550 doublet is present before the second exothermic DSC peak. Therefore, when present, the 550 doublet indicates that the sample has not undergone the recrystallization to orthorhombic L-BS2 as will be discussed below.

In summary, after BS2 cubes have experienced the first peak exothermic peak multiple crystal phases have grown in the supercooled liquid but it is not entirely crystalline. We have identified a significant amount of H-BS2 and minor amounts of B3S5. However, some diffraction peaks remain unexplained and, therefore, it is possible that another phase(s) is present. In addition, the presence of the amorphous halos, albeit small, remain at 875 °C, 0 min. Hence, there is evidence for residual glass after the first exothermic

peak. This residual glass is likely trapped between the fibrillar and spherulitic crystals as inferred from the discrepancy in nucleation rates determined by optical microscopy and diffraction methods.<sup>4</sup> The breadth of features in both Raman spectra and diffractograms are also indicative of fine spherulitic or fibrillar growth and suggests that these crystals may be somewhat distorted or contain defects.

#### 4.2 Why do non-stoichiometric barium silicate phases and H-BS2 form at low temperatures?

Structurally, the barium silicate minerals of compositions from  $\text{BaSiO}_3$  to  $\text{Ba}_3\text{Si}_5\text{O}_{13}$  are composed of single zweier chains with multiplicities of 1 to 5; they form from single chains, multiplicity of 1 (H-BS), to ribbons of 3 (B2S3), 4 (B5S8), and 5 (B3S5) chains joined together. The BS2 polymorphs are composed of sheets of tetrahedra that can also be described as an infinite number of chains; multiplicity equals  $\infty$ .<sup>45</sup> If the liquid barium disilicate starts as a random network which crystallizes into sheets than it must also be capable of first forming chains of varying multiplicity. Thus, the possibility of crystallizing non-stoichiometric phases from the SCL BS2 may in fact be the rule rather than the exception where such structures are stable in the binary, even if only in minor concentrations ( $\sim 1\%$ ).

The issue remains of how H-BS2 is formed at low temperatures ( $\sim 700\text{--}900\text{ °C}$ ), much below where it is thermodynamically stable ( $>1350\text{ °C}$ ). As pointed out by several authors, the phase transition from either L-BS2 or H-BS2 to the other is a reconstructive one.<sup>12,45</sup> The sheets of  $\text{SiO}_4$  within either L-BS2 or H-BS2 are composed of tetrahedral pairs having either the same or opposing orientations. In pairs with the same orientation, both tetrahedra have their terminal oxygen (non-bridging oxygen) pointing in the same direction. In pairs with the opposing orientation, one tetrahedron points in the



positive and one in the negative directions. H-BS2 has tetrahedral pairs with both orientations, whereas, in L-BS2 all tetrahedral pairs have the same orientation. As a result, the configurational entropy of H-BS2 is lower than that of L-BS2 despite its higher temperature of formation.<sup>12</sup> Although the configurational energy is lower in H-BS2 than in L-BS2, the overall energetic differences between the corrugated sheets of H-BS2 is compensated by the flat (and more symmetric) sheets found in L-BS2 resulting in it being the equilibrium phase at low temperatures.<sup>12</sup> In contrast, the BS2 glass network has a range of SiO<sub>4</sub> connectivities, from Q<sup>2</sup> to Q<sup>4</sup>, with an isotropic distribution (e.g. ref. 25 and 46). Thus, two structural reasons are found to explain the presence of H-BS2 at low temperatures. Because it does not have to align all of the tetrahedra, nor do the SiO<sub>4</sub> sheets have to be completely flat. Therefore, we suggest that this lower configurational entropy is the key to explaining why H-BS2 is formed in the early stages of crystallization of barium disilicate glasses.

#### 4.3 What is the origin of the 2<sup>nd</sup> DSC peak?

There is remarkable agreement in both the XRD and Raman results for samples that have experienced the second exothermic DSC peak. All results indicate that the heat treatments that surpass the second peak (e.g. 5 min at 875 °C or 905 °C) form orthorhombic L-BS2 (sanbornite) (Fig. 2 and 3). This is confirmed by Rietveld analysis of the diffractograms (e.g. Fig. 8; ESI† Fig. S1). As noted above, L-BS2 is characterized by an intense diffraction peak at 22.4° ([011]), as well as, the distinct doublet at 33° 2θ (the [401] and [221] planes) (Fig. 3B). Although the 853 °C sample retains <1% B3S5 after 60 min, Rietveld analysis shows that it is 99% L-BS2 (ESI† Fig. S1). BS2 samples held for five minutes at 875 and 905 °C are also composed entirely of L-BS2 (Fig. 3B). The rapid conversion of these samples to L-BS2 suggests that the non-stoichiometric

phases and residual glass are kinetically trapped. Their role in the crystal nucleation process remains open for debate.

The Raman spectra are consistent with the diffraction results. For example, the 853 °C, 60 min, and the 875 °C, 5 min, samples have spectra comparable to L-BS2 (Fig. 4). The 905 °C, 5 min, likewise is comparable to L-BS2. The distinguishing features of L-BS2 are the small doublet at 330 cm<sup>-1</sup>, the lack of the 550 doublet, and the main peak positions of the Si–O–Si bending and the symmetric stretching modes (Fig. 7). The latter bending and stretching modes have peaks positions found above 531.7 and 1075.2 cm<sup>-1</sup>, respectively, when crystalline L-BS2 is present (Table 1). Clearly, both methods strongly argue that all of the phases found during the first exothermic peak become L-BS2 after second exothermic peak.

However, we observed that the second exothermic peak is actually composite with two peaks that are kinetically distinct (Fig. 2). As the first exothermic peak involves H-BS2, B3S5, residual glass, possibly L-BS2 and another phase, there are multiple routes involved in the formation of L-BS2. Therefore, at least three steps are required to complete this recrystallization: a) first, the residual glass must crystallize; b) second, any non-stoichiometric phases must convert to a BS2 phase; and, c) third, there must be a phase transition from H-BS2 to L-BS2. In either case, the residual glass and non-stoichiometric phases must both be consumed to reach the BS2 composition. Therefore, the two local maxima of the second exothermic peak may be assigned to the crystallization of the residual glass and non-stoichiometric phase(s), and to the high-to-low phase transition of crystalline BS2.

The introduction of this work highlighted the fact that other important glass-forming systems (e.g. Ba<sub>2</sub>TiSi<sub>2</sub>O<sub>8</sub>, CaMgSi<sub>2</sub>O<sub>6</sub>) also display two exothermic peaks in their calorimetry measurements. In the latter case, in CaMgSi<sub>2</sub>O<sub>6</sub> glass, the origin of the second peak appears to be related to the phase transition of diopside to a wollastonite-like structure which was shown to form under tension.<sup>8</sup> Although strong evidence is presented in ref. 8, diopside is not known to have a wollastonite-like structure. Moreover, structurally, these two phases do not have many intermediate composition phases.<sup>45</sup> Therefore, given these peculiarities, the difference in compositions, and in structures, these exothermic peaks should each be investigated to determine their origins.

## 5 Conclusions

For a slightly hyper-stoichiometric BS2 glass heated at 10 °C min<sup>-1</sup>, the first exothermic peak is related to the formation of H-BaSi<sub>2</sub>O<sub>5</sub>, Ba<sub>3</sub>Si<sub>5</sub>O<sub>13</sub>, possibly L-BaSi<sub>2</sub>O<sub>5</sub> and another unknown phase. However, the existence of the sharp exothermic peak does not necessarily indicate evidence for complete crystallization as some residual glass is observed in the X-ray diffraction patterns. The second exothermic peak is actually composed of two peaks, which are typically not addressed in most calorimetry-based works. In the second exothermic peak, there are multiple processes including crystallization of

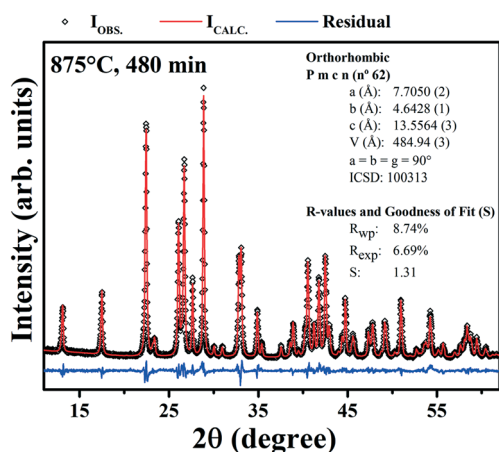


Fig. 8 Rietveld refinement of BS2 sample after isothermal treatment of 480 min at 875 °C ( $R_{wp} = 8.74\%$ ;  $R_{exp} = 6.69\%$ ;  $\chi^2 = 1.31$ ). The sample has completely crystallized to orthorhombic L-BS2. The same is true for all 480 min samples except the lowest most temperature, 853 °C, which contains minor (<1%) Ba<sub>3</sub>Si<sub>5</sub>O<sub>13</sub>. The Rietveld refinement fit is the solid red line whereas the lower, solid blue line is the residual.

the residual glass, recrystallization of non-stoichiometric phases to BS2 and the phase transition of monoclinic H-BaSi<sub>2</sub>O<sub>5</sub> to orthorhombic L-BaSi<sub>2</sub>O<sub>5</sub>.

This low temperature phase transition is the opposite of that expected at 1350 °C, where L-BaSi<sub>2</sub>O<sub>5</sub> converts to H-BaSi<sub>2</sub>O<sub>5</sub> as the equilibrium phase. The presence of non-stoichiometric phases is also exceptional. We suggest that these two aspects may be explained by the structure of chain and sheet barium silicates. The phase transition is promoted by the lower configurational entropy of H-BaSi<sub>2</sub>O<sub>5</sub> due to the variations in orientation of the SiO<sub>4</sub> tetrahedra and the corrugation of the sheets. The evolution of non-stoichiometric phases is promoted by formation of increasing multiplicity of the SiO<sub>4</sub> chains (e.g. Ba<sub>3</sub>Si<sub>5</sub>O<sub>13</sub>) until they form an infinite sheet (e.g. H-BaSi<sub>2</sub>O<sub>5</sub>) from the random silicate network in the supercooled liquid. The kinetics of the above changes are sensitive to the sample mass, heating rate, and the degree of undercooling.

Therefore, if these relationships are further constrained, it may be possible to custom design barium silicate glass-ceramics with a given barium silicate phase. This could be important for the design of barium silicate glass-ceramics with specific mechanical and optical properties. Finally, these original results highlight the fact that other important glass-forming systems (e.g. Ba<sub>2</sub>TiSi<sub>2</sub>O<sub>8</sub>) also display two exothermic peaks in their calorimetry measurements and warrant further investigation.

## Conflicts of interest

There are no conflicts to declare.

## Acknowledgements

BJAM and DVS would like to thank the São Paulo Research Foundation (FAPESP) for funding this research under grant no. 2016/18567-5 and 2016/15962-0. AMR would like to thank the Federal Agency for the Support and Improvement of Higher Education (CAPES), grant number PNP20131474 - 33001014004P9. We appreciate the support of CNPq and CAPES support to PSP, TRC and LDS (Finance Code 001). We thank FAPESP for the CEPID project funding (no. 2013/07793-6). We would like to thank Dr. L. A. Gorelova and Dr. K. Tait (ROM) for providing barium silicate samples.

## References

- M. H. Lewis and G. Smith, Spherulitic growth and recrystallization in barium silicate glasses, *J. Mater. Sci.*, 1976, **11**, 2015–2026.
- A. H. Ramsden and P. F. James, The effects of amorphous phase separation on crystal nucleation kinetics in BaO-SiO<sub>2</sub> glasses - Part 1 General Survey, *J. Mater. Sci.*, 1984, **19**(5), 1406–1419, DOI: 10.1007/BF00563035.
- A. H. Ramsden and P. F. James, The effects of amorphous phase separation on crystal nucleation kinetics in BaO-SiO<sub>2</sub> glasses - Part 2 Isothermal heat treatments at 700° C, *J. Mater. Sci.*, 1984, **19**(9), 2894–2908, DOI: 10.1007/BF01026965.
- E. D. Zanotto and P. F. James, Experimental test of the general theory of transformation kinetics: Homogeneous nucleation in a BaO-2SiO<sub>2</sub> glass, *J. Non-Cryst. Solids*, 1988, **104**(1), 70–72, DOI: 10.1016%2F0022-3093%2888%2990183-4.
- A. M. Rodrigues, J. P. Rino, P. S. Pizani and E. D. Zanotto, Structural and dynamic properties of vitreous and crystalline barium disilicate: Molecular dynamics simulation and Raman scattering experiments, *J. Phys. D: Appl. Phys.*, 2016, **49**(43), 435301, DOI: 10.1088%2F0022-3727%2F49%2F43%2F435301.
- M. Kerstan and C. Rüssel, Barium silicates as high thermal expansion seals for solid oxide fuel cells studied by high-temperature X-ray diffraction (HT-XRD), *J. Power Sources*, 2011, **196**(18), 7578–7584, Available from: <http://linkinghub.elsevier.com/retrieve/pii/S0378775311008755>.
- A. Herrmann, A. Simon and C. Rüssel, Preparation and luminescence properties of Eu<sup>2+</sup>-doped BaSi<sub>2</sub>O<sub>5</sub> glass-ceramics, *J. Lumin.*, 2012, **132**(1), 215–219.
- V. M. Fokin, A. S. Abyzov, J. W. P. Schmelzer and E. D. Zanotto, Stress induced pore formation and phase selection in a crystallizing stretched glass, *J. Non-Cryst. Solids*, 2010, **356**(33–34), 1679–1688.
- A. M. Rodrigues, Estudo da cinética de cristalização em um vidro de fresnoíta dd (2BaO-TiO<sub>2</sub>-2SiO<sub>2</sub>) via DSC/DTA, *M.Sc. Dissertation*, INSTITUTO FEDERAL DE EDUCAÇÃO, CIÊNCIA E TECNOLOGIA DO MARANHÃO, 2010.
- A. M. Rodrigues, J. M. Rivas Mercury, V. S. Leal and A. A. Cabral, Isothermal and non-isothermal crystallization of a fresnoite glass, *J. Non-Cryst. Solids*, 2013, **362**(1), 114–119, DOI: 10.1016/j.jnoncrysol.2012.11.026.
- G. Oehlschlegel, Crystallization of Glasses in the System BaO · 2SiO<sub>2</sub>-2BaO-3SiO<sub>2</sub>, *J. Am. Ceram. Soc.*, 1975, **3–4**, 148–149.
- L. A. Gorelova, R. S. Bubnova, S. V. Krivovichev, M. G. Krzhizhanovskaya and S. K. Filatov, Thermal expansion and structural complexity of Ba silicates with tetrahedrally coordinated Si atoms, *J. Solid State Chem.*, 2016, **235**, 76–84, DOI: 10.1016/j.jssc.2015.12.012.
- Y. Takahashi, H. Masai and T. Fujiwara, Nucleation tendency and crystallizing phase in silicate glasses: A structural aspect, *Appl. Phys. Lett.*, 2009, **95**(071904), 1–3.
- Y. Takahashi, M. Osada, H. Masai and T. Fujiwara, Transmission electron microscopy and in situ Raman studies of glassy sanbornite: An insight into nucleation trend and its relation to structural variation, *J. Appl. Phys.*, 2010, **108**(6), 63507, DOI: 10.1063%2F1.3487473.
- M. C. C. C. Araujo, W. J. Botta, M. J. Kaufmann, R. S. Angelica, J. M. R. R. Mercury and A. A. A. Cabral, Residual glass and crystalline phases in a barium disilicate glass-ceramic, *Mater. Charact.*, 2015, **110**, 192–196, DOI: 10.1016%2Fj.matchar.2015.10.019.
- L. A. Silva, J. M. R. Mercury and A. A. Cabral, Determining the Crystal Volume Fraction of BS2 Glass by Differential Scanning Calorimetry and Optical Microscopy, *J. Am. Ceram. Soc.*, 2013, **96**(1), 130–136, DOI: 10.1111/jace.12097.

- 17 A. M. Rodrigues, Processos difusionais, cristalização e escoamento viscoso em disilicato de bário vítreo, *Ph.D. Dissertation*, Universidade Federal de São Carlos, 2014.
- 18 X. Xia, I. Dutta, J. C. Mauro, B. G. Aitken and K. F. Kelton, Temperature dependence of crystal nucleation in BaO-2SiO<sub>2</sub> and 5BaO-8SiO<sub>2</sub> glasses using differential thermal analysis, *J. Non-Cryst. Solids*, 2017, **459**, 45–50.
- 19 G. Oehlschlegel, Crystallization of glasses in the system BaO·2SiO<sub>2</sub>-2BaO-3SiO<sub>2</sub>, *J. Am. Ceram. Soc.*, 1975, **58**(3–4), 148–148, DOI: 10.1111/j.1151-2916.1975.tb19584.x.
- 20 V. M. Fokin, E. D. Zanotto and J. W. P. Schmelzer, Homogeneous nucleation versus glass transition temperature of silicate glasses, *J. Non-Cryst. Solids*, 2003, **321**(1–2), 52–65, DOI: 10.1016/S0022-3093(03)00089-9.
- 21 V. M. Fokin, E. D. Zanotto, N. S. Yuritsyn and J. W. P. Schmelzer, Homogeneous crystal nucleation in silicate glasses: A 40 years perspective, *J. Non-Cryst. Solids*, 2006, **352**(26–27), 2681–2714, DOI: 10.1016%2Fj.jnoncrysol.2006.02.074.
- 22 J. Schneider, V. R. Mastelaro, E. D. Zanotto, B. A. Shakhmatkin, N. M. Vedishcheva and A. C. Wright, *et al.* Q<sup>n</sup> distribution in stoichiometric silicate glasses: thermodynamic calculations and <sup>29</sup>Si high resolution NMR measurements, *J. Non-Cryst. Solids*, 2003, **325**(1–3), 164–178, DOI: 10.1016/S0022-3093(03)00332-6.
- 23 E. D. Zanotto, J. E. Tsuchida, J. F. Schneider and H. Eckert, Thirty-year quest for structure-nucleation relationships in oxide glasses, *Int. Mater. Rev.*, 2015, **60**(7), 376–391, DOI: 10.1080/09506608.2015.1114706.
- 24 A. M. Rodrigues, D. R. Cassar, V. M. Fokin and E. D. Zanotto, Crystal growth and viscous flow in barium disilicate glass, *J. Non-Cryst. Solids*, 2018, **479**, 55–61, DOI: 10.1039/c7ce02135f.
- 25 B. J. A. Moulton, A. M. Rodrigues, P. S. Pizani, D. V. Sampaio and E. D. Zanotto, A Raman investigation of the structural evolution of supercooled liquid barium disilicate during crystallization, *Int. J. Appl. Glass Sci.*, 2018, **9**(4), 510–517, DOI: 10.1111/ijag.12356.
- 26 M. Wojdyr, Fityk: A general-purpose peak fitting program, *J. Appl. Crystallogr.*, 2010, **43**(5 PART 1), 1126–1128.
- 27 H. M. Rietveld, Line profiles of neutron powder-diffraction peaks for structure refinement, *Acta Crystallogr.*, 1967, **22**(1), 151–152, Available from: <http://scripts.iucr.org/cgi-bin/paper?S0365110X67000234>.
- 28 A. C. Larson and R. B. Von Dreele, *General Structure Analysis System (GSAS)*, Los Alamos Natl Lab Rep LAUR, 2004, vol. 748, pp. 86–748, Available from: <https://subversion.xor.aps.anl.gov/EXPGUI/gsas/all/GSAS Manual.pdf>.
- 29 L. B. McCusker, R. B. Von Dreele, D. E. Cox, D. Louër and P. Scardi, Rietveld refinement guidelines, *J. Appl. Crystallogr.*, 1999, **32**(1), 36–50.
- 30 K. F. Hesse and F. Liebau, Crystal chemistry of silica-rich Barium silicates I: Refinement of the crystal structures of Ba<sub>4</sub>[Si<sub>6</sub>O<sub>16</sub>], Ba<sub>5</sub>[Si<sub>8</sub>O<sub>21</sub>] and Ba<sub>6</sub>[Si<sub>10</sub>O<sub>26</sub>], silicates with triple, quadruple and quintuple chains, *Z. Kristallogr. - New Cryst. Struct.*, 1980, **153**(1–2), 3–17.
- 31 K. F. Hesse and F. Liebau, Crystal chemistry of silica-rich Barium silicates III: Refinement of the crystal structures of the layer silicates Ba<sub>2</sub>[Si<sub>4</sub>O<sub>10</sub>] (I), (Sanbornite), and Ba<sub>2</sub>[Si<sub>4</sub>O<sub>10</sub>] (h), *Z. Kristallogr.*, 1980, **153**(1–2), 33–41, DOI: 10.1524%2Fzkri.1980.153.14.3.
- 32 A. M. Rodrigues, L. D. Silva, R. Zhang and V. O. Soares, Structural effects on glass stability and crystallization, *CrystEngComm*, 2018, **20**(16), 2278–2283.
- 33 A. M. Rodrigues, J. L. L. Narváez-Semanate, A. A. Cabral and A. C. M. Rodrigues, Determination of crystallization kinetics parameters of a Li<sub>1.5</sub>Al<sub>0.5</sub>Ge<sub>1.5</sub>(PO<sub>4</sub>)<sub>3</sub> (LAGP) glass by differential scanning calorimetry, *Mater. Res.*, 2013, **16**(4), 811–816.
- 34 E. D. Zanotto, The Effects of Amorphous Phase Separation on Crystal Nucleation in Baria-Silica and Lithia-Silica Glasses, *Ph.D. Dissertation*, University of Sheffield, 1982.
- 35 O. Russina, A. Triolo, L. Gontrani and R. Caminiti, Mesoscopic structural heterogeneities in room-temperature ionic liquids, *J. Phys. Chem. Lett.*, 2012, **3**(1), 27–33.
- 36 T. A. Lima, V. H. Paschoal, L. F. O. Faria and M. C. C. Ribeiro, Unraveling the Stepwise Melting of an Ionic Liquid, *J. Phys. Chem. B*, 2017, **121**(17), 4650–4655.
- 37 L. Cormier, P. H. Gaskell and S. Creux, Comparison of the low-Q features in diffraction data for silicate glasses and crystals containing Sr or Ba, *J. Non-Cryst. Solids*, 1999, **248**(1), 84–91.
- 38 P. H. Gaskell, Relationships between the medium-range structure of glasses and crystals, *Mineral. Mag.*, 2000, **64**(3), 425–434, DOI: 10.1180/002646100549481.
- 39 S. W. Kieffer, Thermodynamics and lattice vibrations of minerals: 1. Mineral heat capacities and their relationships to simple lattice vibrational models, *Rev. Geophys.*, 1979, **17**, 1–19, DOI: 10.1029/RG017i001p00001.
- 40 P. McMillan, Structural studies of silicate glasses and melts—applications and limitations of Raman spectroscopy, *Am. Mineral.*, 1984, **69**(7–8), 622–644.
- 41 M. S. Bradley, Lineshapes in IR and Raman Spectroscopy: A Primer, *Spectroscopy*, 2015, vol. 30(11), pp. 42–46, Available from: <http://www.spectroscopyonline.com/lineshapes-ir-and-raman-spectroscopy-primer>.
- 42 P. McMillan, Structural studies of silicate glasses and melts—applications and limitations of Raman spectroscopy, *Am. Mineral.*, 1984, **69**(7–8), 622–644.
- 43 S. A. Brawer and W. B. White, Raman spectroscopic investigation of the structure of silicate glasses: I. The binary alkali silicates, *J. Chem. Phys.*, 1975, **63**(6), 2421–2432.
- 44 M. Tribaudino, L. Mantovani, D. Bersani and P. P. Lottici, Raman spectroscopy of (Ca,Mg)MgSi<sub>2</sub>O<sub>6</sub> clinopyroxenes, *Am. Mineral.*, 2012, **97**(8–9), 1339–1347, DOI: 10.2138/am.2012.4057.
- 45 F. Liebau, *Structural Chemistry of Silicates*, New York, Springer-Verlag, 1st edn, 1985, p. 347.
- 46 H. Schlenz, A. Kirfel, K. Schulmeister, N. Wartner, W. Mader and W. Raberg, *et al.* Structure analyses of Ba-silicate glasses, *J. Non-Cryst. Solids*, 2002, **297**(1), 37–54, DOI: 10.1016/S0022-3093(01)00922-X.